Electronic Supplementary Information (ESI) for:

Nanostructuring polymers with high surface area using inorganic templates for efficient extraction of anionic dyes from solutions

Tao Zhang,[a] Xiaoxi Huang,[b] and Tewodros Asefa[*abc]

[a] Department of Chemical and Biochemical Engineering, Rutgers, The State University of New Jersey, 98 Brett Road, Piscataway, New Jersey 08854, USA.

[b] Department of Chemistry and Chemical Biology, Rutgers, The State University of New Jersey, 610 Taylor Road, Piscataway, New Jersey 08854, USA.

[c] Institute of Advanced Materials, Devices and Nanotechnology, Rutgers, The State University of New Jersey, Piscataway, New Jersey 08854, USA.

[*] E-mail: tasefa@rci.rutgers.edu

Table of Contents

1. Detailed Experimental Section

1.1. Materials and reagents

Poly(ethylene glycol)-*block*-poly(propylene glycol)-*block*-poly(ethylene glycol) ($(PEG)_{20}(PPG)_{70}(PEG)_{20}$ or Pluronic® 123) was obtained from BASF. Tetraethyl orthosilicate (TEOS), aniline, ammonium persulfate, hydrochloric acid (ACS Reagent, 37%), ammonium hydroxide, and Orange G (OG) were purchased from Sigma-Aldrich. Anhydrous ethanol was received from Fischer Scientific. Deionized water was used in all the experiments.

1.2. Synthesis of SBA-15 mesoporous silica

First, 4 g Pluronic® 123 was mixed with a solution containing 20 mL concentrated hydrochloric acid and 130 mL deionized water, and the solution was stirred at 45 °C. After the Pluronic® 123 was dissolved completely, 8.5 g TEOS was added drop-wise into the solution. The solution was vigorously stirred at 45 °C for 20 h, and then kept in oven at 80 °C for 24 h under static condition. The solution was filtered, and the resulting white precipitate was washed copiously with deionized water and dried at 60 °C in oven, giving the as-synthesized SBA-15. The as-synthesized SBA-15 was then calcined at 550 °C for 5 h to remove the Pluronic®123 templates in it. This finally resulted in the desired mesoporous SBA-15 material.

1.3. Synthesis of H^+-PANI/SBA-15 and PANI/SBA-15

First, 150 mg SBA-15 was dispersed uniformly in 30 mL deionized water by sonication. Then, 0.3 mL (3.28 mmol) of aniline was added to the above suspension, and the mixture was stirred for 4 h at room temperature. After adjusting the suspension's pH to 4 by adding some hydrochloric acid (1 M), the mixture was stirred for another 4 h in an ice bath (0-5 °C) to let the protonated aniline disperse uniformly. Into the above

suspension, a solution prepared by dissolving 750 mg ammonium persulfate (3.28 mmol) in 1 mL deionized water was slowly added drop-wise. The polymerization of aniline, forming polyaniline (PANI), then started to take place immediately, as indicated by the change in color of the dispersion from white to dark green. The polymerization was let to go for 10 h. The solid product (H^+-PANI/SBA-15) was then collected by centrifugation and washed with copious amount of deionized water and ethanol until the supernatant became clear. The resulting solid product was the emeraldine salt form of PANI supported onto SBA-15, named H^+-PANI/SBA-15.

For comparative studies, PANI/SBA-15 (the emeraldine base form of PANI supported onto SBA-15) was also synthesized. This was done by stirring 20 mg H^+-PANI/SBA-15 in 40 mL aqueous ammonia solution (0.01 M) for 4 h, and then centrifugation of the suspension and washing the recovered precipitate *via* sonication with ethanol, followed by centrifugation and decantation. The color of the sample changed from dark green to dark blue, indicating the transformation of H^+-PANI/SBA-15 to PANI/SBA-15.

1.4. Synthesis of H^+-PANI and PANI

To synthesize H^+-PANI, 1 mL (11 mmol) of aniline was mixed with 100 mL deionized water and the solution was stirred for 4 h at room temperature. The pH of the solution was adjusted to 4 by adding some hydrochloric acid (1 M) into it. The solution was further stirred for another 4 h in an ice bath (0-5 °C) to let the protonated aniline disperse uniformly. Then, 2.5 g ammonium persulfate (11 mmol) was dissolved in 1 mL deionized water and slowly added, drop-wise, to the above suspension, to initiate the polymerization of aniline. The polymerization reaction was let to go for 10 h. The green solid product, which was recovered *via* centrifugation, was washed with deionized water, followed by ethanol. This resulted in the hydrochloric acid-doped PANI, or H^+-PANI.

For comparative studies, the undoped form of H^+-PANI (or PANI) was also

synthesized by treating 20 mg H^+-PANI with 40 mL ammonia solution (0.01 M) for 4 h, and then washing the resulting polymer with ethanol and recovering it from the solution *via* centrifugation, followed by decantation.

1.5. Standard curves for concentration of Orange G (OG) versus absorbance

The absorbance of different concentrations (2, 4, 5, 10, 15, 20, 30, and 40 μg/mL) of OG in both PBS and deionized water was measured by UV-Vis spectroscopy in the range of 300 nm to 800 nm. The absorption maximum for OG occurs at 480 nm, and by using the band's intensity at this wavelength, the correlation between intensity and concentration of OG with the Beer-Lambert equation was determined. Specifically, two equations, one for water and another for PBS, were obtained and then used to calculate the amount of OG adsorbed by the materials in the adsorption experiments.

1.6. Characterizations and instrumentations

Transmission electron microscope (TEM) images were taken with a Topcon 002B TEM microscope operating at 200 KV. Scanning electron microscopic (SEM) images were obtained using a Zeiss Sigma field emission scanning electron microscope (FESEM). UV-Vis spectra (including solid UV-Vis) were acquired with a Lambda 950 spectrophotometer (PerkinElmer). Nitrogen adsorption-desorption isotherms were performed using a Micromeritics Tristar-3000 instrument. The sample was degassed at 333 K for 8 h under a flow of nitrogen gas before each measurement. From the adsorption isotherms and data, the surface area and pore size distributions of the materials were determined by Brunauer-Emmett-Teller (BET) method and Barrett-Joyner-Halenda (BJH) method, respectively. pH values of solutions were determined with Accumet pH meter 915 (Fisher Scientific). FTIR spectra were recorded using a Thermo Nicolet Avatar 360 FTIR spectrometer. Thermogravimetric analyses (TGA) of the materials were performed on PerkinElmer TGA7 instrument.

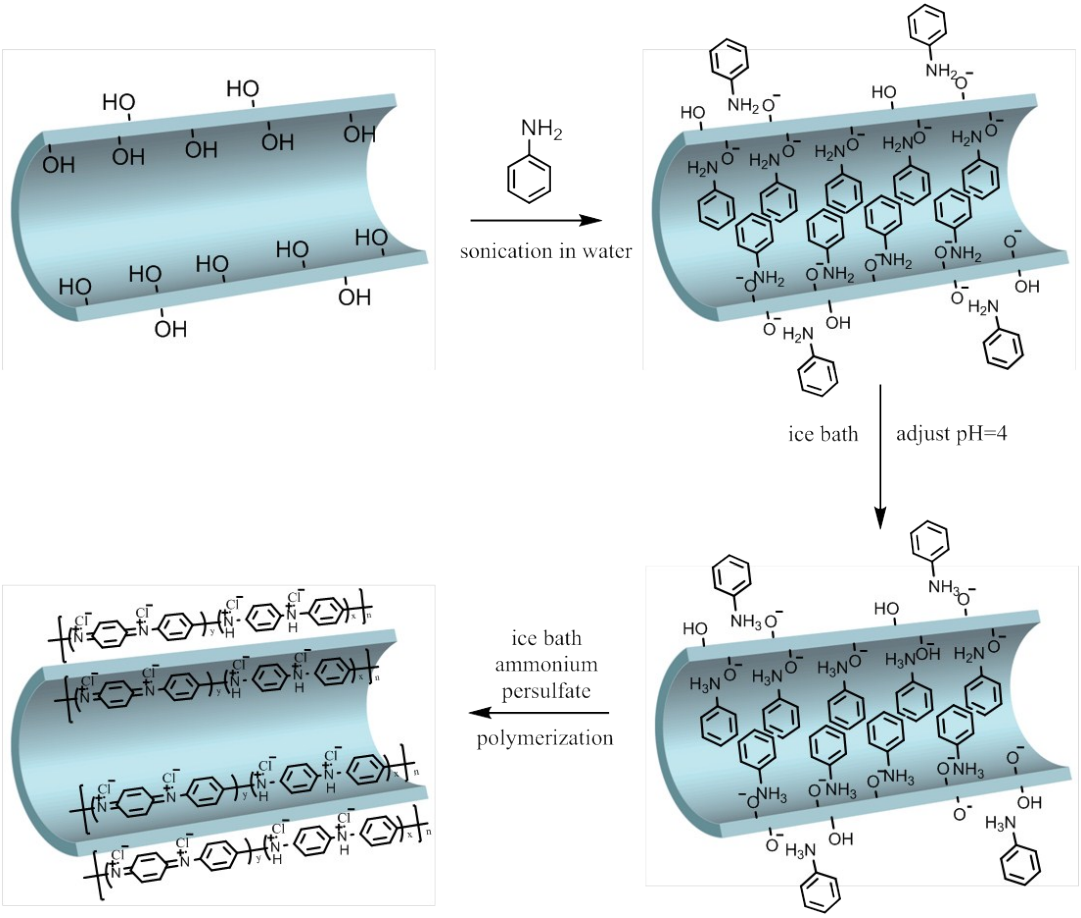

Fig. S1. Schematics of the synthesis of H^+-PANI/SBA-15 material.[1]

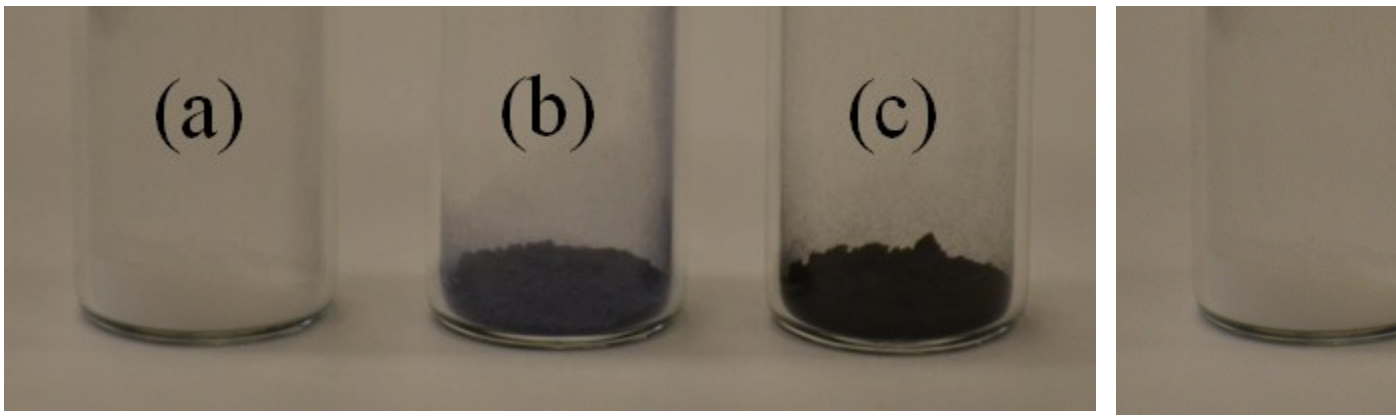

Fig. S2. Photographs of SBA-15 (white color) (a), PANI/SBA-15 (dark blue) (b), and H^+-PANI/SBA-15 (dark green) (c).

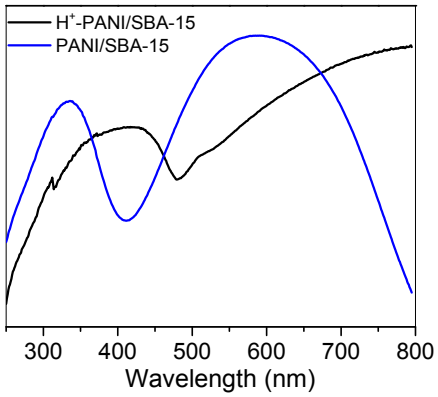

Fig. S3. Diffuse UV-Vis spectra of H^+-PANI/SBA-15 and PANI/SBA-15.

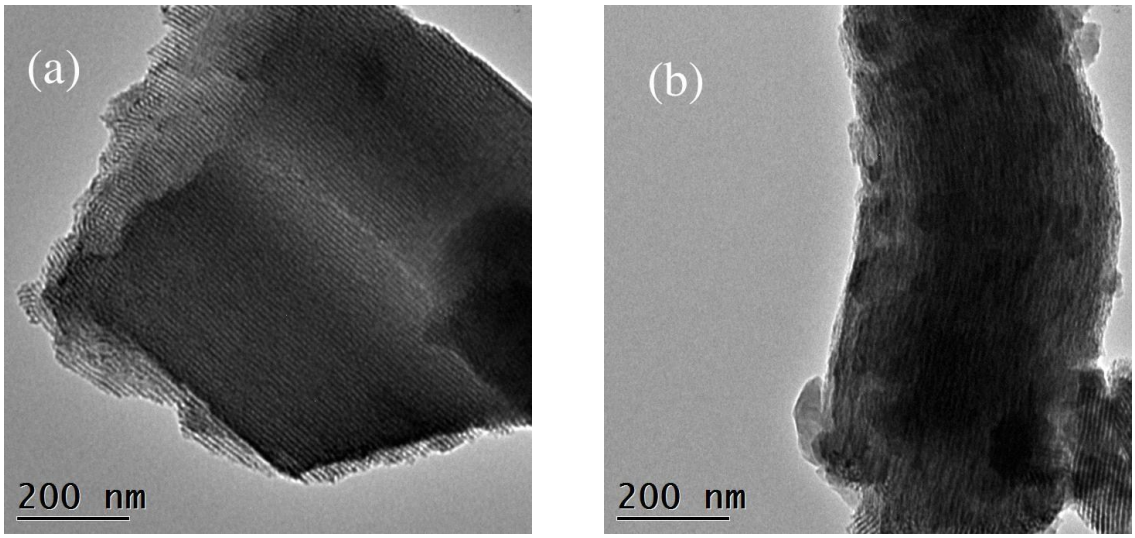

Fig. S4. TEM images of SBA-15 (a) and H^+-PANI/SBA-15 (b).

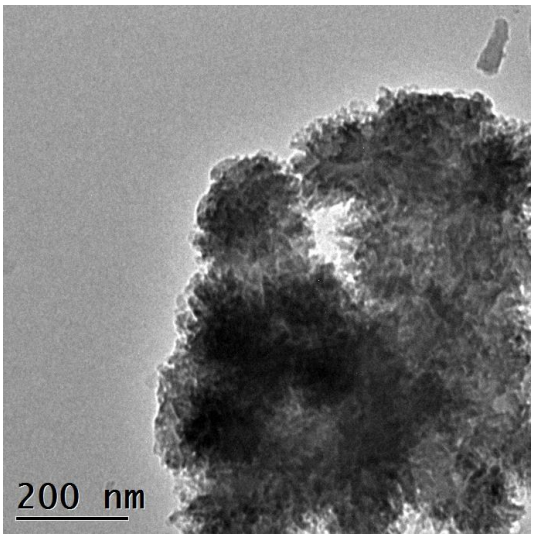

Fig. S5. TEM image of H^+-PANI.

Fig. S6. SEM images of SBA-15 (a) and H^+-PANI/SBA-15 (b). The SEM images of H^+-PANI/SBA-15 show rod-like morphology akin to that of SBA-15, the material used as a template. Moreover, the surfaces of H^+-PANI/SBA-15 appear rougher than those of SBA-15, suggesting that the outer surfaces of the SBA-15 particles in the former most likely possess PANI.

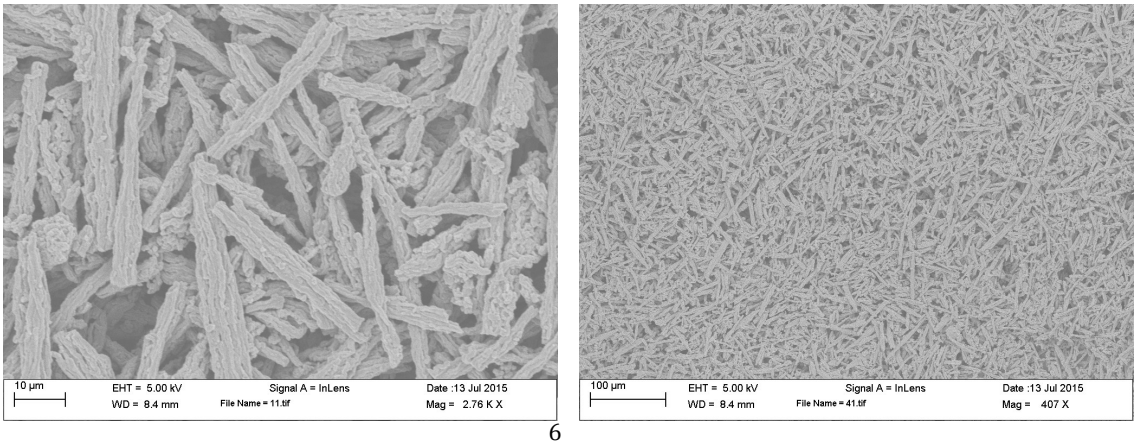

Fig. S7. Lower magnification SEM images of H^+-PANI/SBA-15. The particles were recovered after centrifugation and washing (following a procedure similar to the one used to collect the H^+-PANI shown in Fig. S5). As no isolated polymeric particles were observed in the images, the images confirm that the polymerization process has occurred mainly on the surfaces of SBA-15, or barely in the solution.

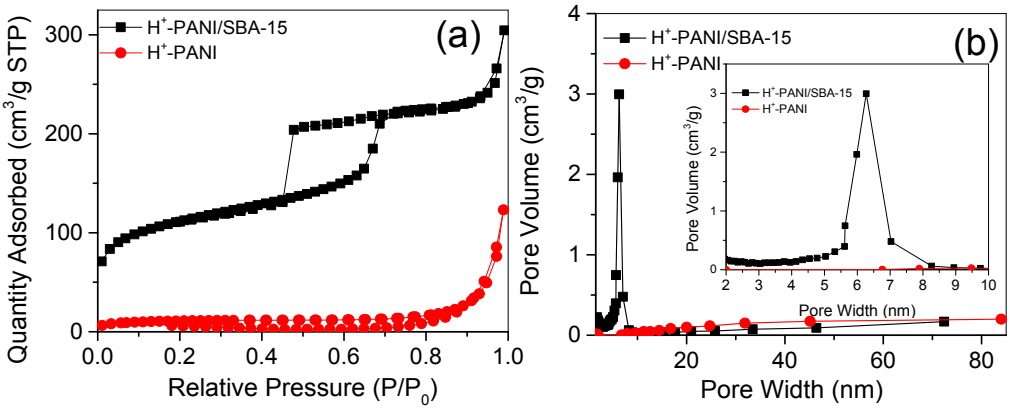

Fig. S8. (a) N_2 adsorption/desorption isotherms and (b) pore size distributions of H^+-PANI/SBA-15 and H^+-PANI materials.

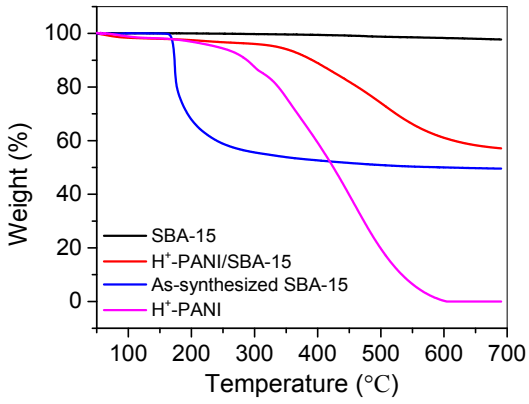

Fig. S9. TGA curves of as-synthesized SBA-15, SBA-15, H^+-PANI, and H^+-PANI/SBA-15.

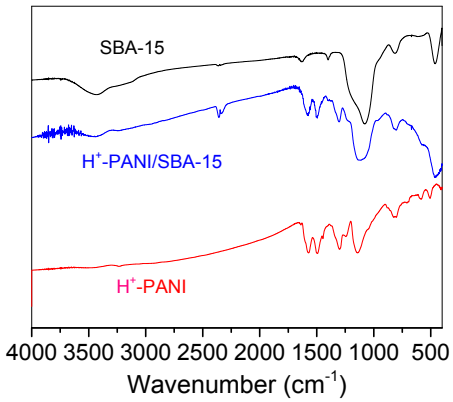

Fig. S10. FTIR spectra of SBA-15, H^+-PANI, and H^+-PANI/SBA-15.

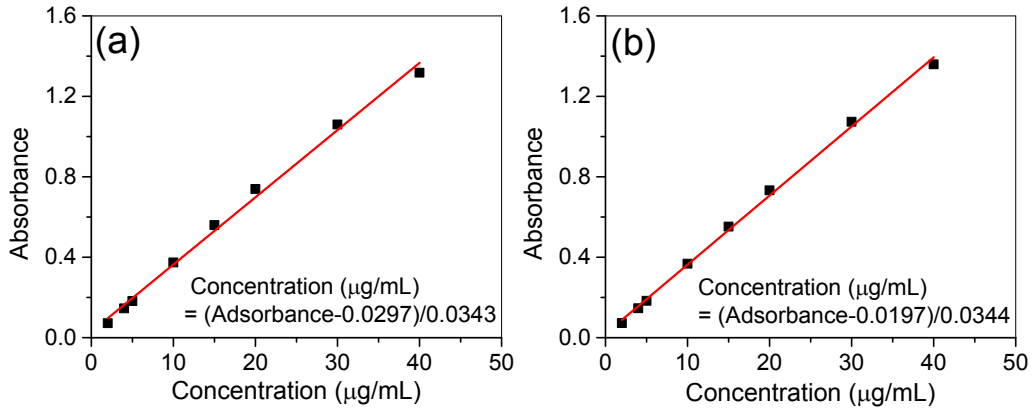

Fig. S11. Standard curves based on the absorbance of the absorption maximum of OG at 480 nm versus concentration of OG in PBS (a) and distilled water (b).

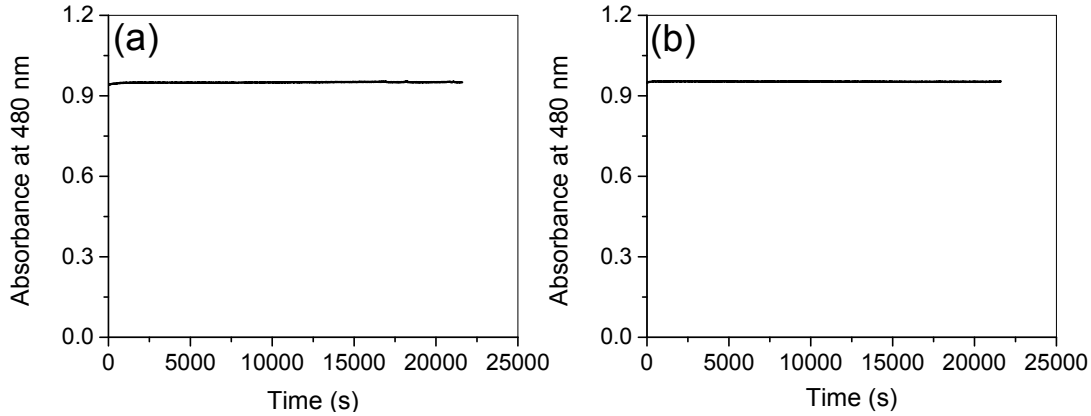

Fig. S12. Absorbance of 25 μg/mL OG at 480 nm in PBS (a) and distilled water (b) measured for 6 h.

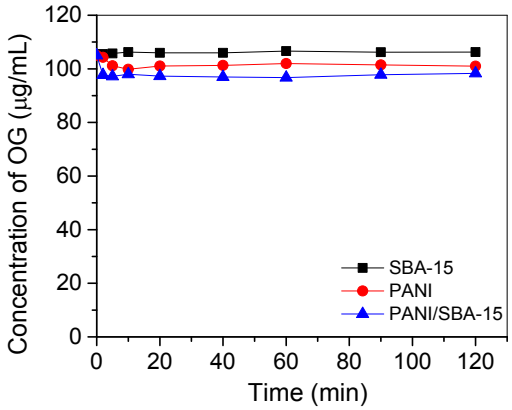

Fig. S13. Concentration profiles of OG over 2 h in the presence of SBA-15, PANI and PANI/SBA-15 in PBS.

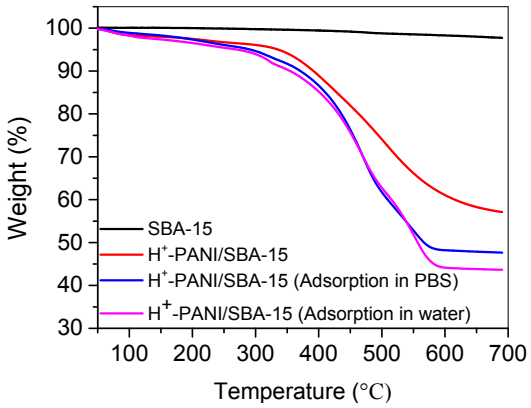

Fig. S14. Thermogravimetric analysis (TGA) curves of OG-saturated SBA-15, H^+-PANI/SBA-15, OG-saturated H^+-PANI/SBA-15 in PBS, and OG-saturated H^+-PANI/SBA-15 in water.

Using the results in the TGA traces in Fig. S14, the amount of OG in OG-saturated H^+-PANI/SBA-15 from PBS or aqueous OG solutions was determined. The TGA traces display that the weight loss from OG-saturated H^+-PANI/SBA-15 in PBS is 52.34%, whereas that from OG-saturated H^+-PANI/SBA-15-OG in water is slightly higher (56.34%). Further calculations show that the amount of OG adsorbed in PBS and distilled water is 201 μg/mg and 310 μg/mg, respectively. The results clearly confirmed that the adsorption capacity of H^+-PANI/SBA-15 is higher in water than in PBS, most likely due to the fact that the PANI backbone remains H^+-doped and more positively charged in former than in the latter.

2. Details of Kinetic and Modeling Studies and Results and Discussions

To study the kinetic behavior of the adsorption of OG in H^+-PANI and H^+-PANI/SBA-15 in both PBS and distilled water, the amount of adsorbent was set at 1 mg/mL in the initial OG concentration of 430 μg/mL at room temperature.

The amount of OG adsorbed at equilibrium q_e (μg/mg) on the adsorbents was then calculated with the following equation:

$$q_e = \frac{(C_0 - C_e)V}{W} \quad (1)$$

where C_0 and C_e (μg/mL) are the liquid phase adsorbate concentration at initial time and at equilibrium, respectively, V is the volume of the solution (mL) and W is the mass of adsorbent used (mg).

The amount of adsorbate in the adsorbent at time t, q_t was calculated by:

$$q_t = \frac{(C_0 - C_t)V}{W} \quad (2)$$

where C_0 and C_t (μg/mL) are the liquid phase adsorbate concentration at initial time and at time t, respectively, V is the volume of the solution (mL) and W is the mass of adsorbent used (mg).

To determine the process by which OG is adsorbed in the materials, pseudo-first order, pseudo-second order and intraparticle diffusion models were tested on the adsorption data obtained for OG on the H^+-PANI/SBA-15 as well as the control materials, and the validity of the models was checked by linear equation analysis of $log(q_e - q_t)\ vs\ t$, $t/q_t\ vs\ t$, and $q_t\ vs\ t^{0.5}$ and their corresponding correlation coefficients, R^2.

2.1. Pseudo-first order

The pseudo-first order rate expression can be given by Lagergren equation[2] in the form of:

$$\frac{dq_t}{dt} = k_1(q_e - q_t) \quad (3)$$

where q_e and q_t (μg/mg) refer to the solid phase adsorbate concentration at equilibrium and at time t (min), respectively, and k_1 is the rate constant of pseudo-first order adsorption (min^{-1}). Integrating equation (3) with boundary conditions at $t = 0$, $q_t = 0$ and $t = t$, $q_t = q_t$, results in:

$$\log (q_e - q_t) = log q_e - \frac{k_1 t}{2.303} \quad (4)$$

2.2. Pseudo-second order

The pseudo-second order kinetic rate equation is expressed as:[3]

$$\frac{dq_t}{dt} = k_2 (q_e - q_t)^2 \quad (5)$$

where q_e and q_t (μg/mg) have the same meaning as in equation (3), and k_2 is the rate constant of pseudo-second order adsorption (mg/μg min). After integrating and rearranging equation (5) using the boundary conditions $t = 0$ to $t = t$ and $q_t = 0$ to $q_t = q_t$, the following equation (Eqn. 6) can be obtained:

$$\frac{t}{q_t} = \frac{1}{k_2 q_e^2} + \frac{t}{q_e} \quad (6)$$

If pseudo-second order kinetics is applicable, the plot of $t/q_t \; vs \; t$ should give a linear relationship, and there is no need to know any parameter beforehand to determine q_e and k_2 (or they can be determined from the slope and intercept of the plot, respectively).

2.3. Intraparticle diffusion model

The third model, intraparticle diffusion model, which was designed by Weber and Morris, is shown in equation (7), and it was also tested on our data.[2,4]

$$q_t = k_i t^{0.5} + C \quad (7)$$

where k_i is the intraparticle diffusion rate constant in μg/mg min$^{0.5}$ and C is a y-intercept (μg/mg), which is proportional to the boundary layer thickness. If the intraparticle diffusion is the rate-controlling factor, then the plot of $q_t \; vs \; t^{0.5}$ should be linear. Moreover, if the plot passes through the origin, then the intraparticle diffusion can be said

to be the only rate-limiting factor.

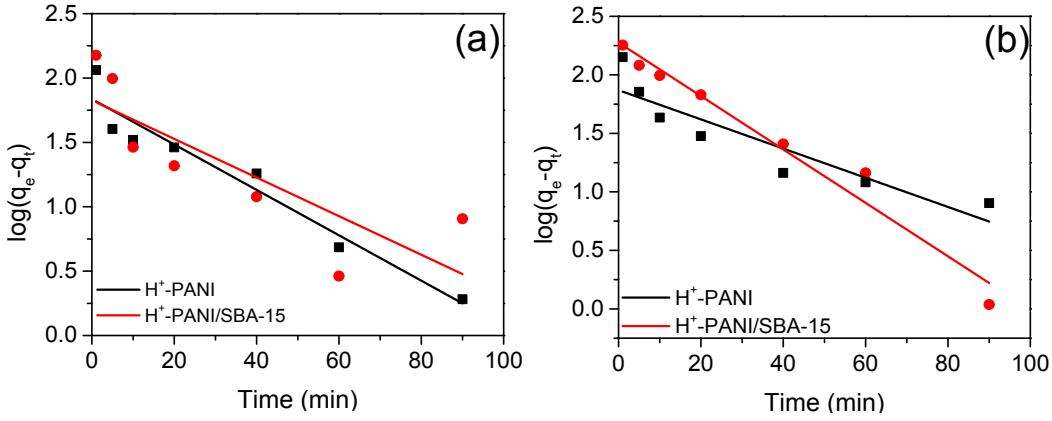

Fig. S15. Pseudo-first order model-based plots of the adsorption of OG in H^+-PANI and H^+-PANI/SBA-15 in PBS (a) and distilled water (b).

Table S1. Comparison of the pseudo first and second order adsorption rate constants ($k_1$and k_2) and experimental and calculated values of q_e for adsorption of OG by H^+-PANI and H^+-PANI/SBA15 in PBS and distilled water.

	First order kinetic model				**Second order kinetic model**		
	q_e **(exp)** **(µg/mg)**	k_1 **(min^{-1})**	q_e **(cal)** **(µg/mg)**	R^2	k_2 **(mg/µg min)**	q_e **(cal)** **(µg/mg)**	R^2
Adsorption in PBS							
H^+-PANI	130.61	4.06 x 10^{-2}	68.64	0.930	1.28 x 10^{-3}	136.42	0.998
H^+-PANI/SBA-15	241.60	3.45 x 10^{-2}	67.17	0.611	1.81 x10^{-3}	243.90	0.999
Adsorption in water							
H^+-PANI	216.72	2.87 x 10^{-2}	73.96	0.810	1.75 x 10^{-3}	216.45	1
H^+-PANI/SBA-15	367.68	5.26 x 10^{-2}	188.54	0.962	8.08 x 10^{-4}	377.36	0.999

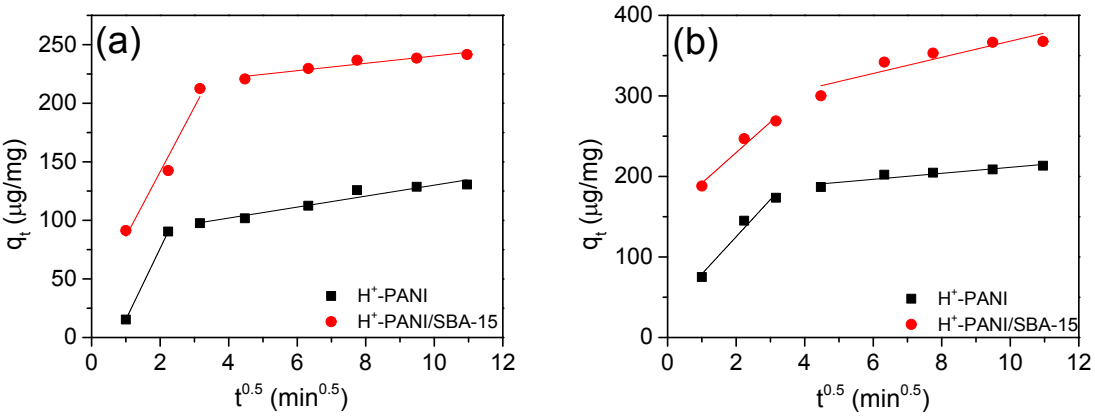

Fig. S16. Intraparticle diffusion model-based plots of adsorption of OG by H^+-PANI and H^+-PANI/SBA-15 in PBS (a) and distilled water (b).

Table S2. Kinetic data of intraparticle diffusion model of OG adsorption by H^+-PANI and H^+-PANI/SBA15 in PBS and distilled water.

	Intraparticle diffusion model			
	k_{i1}	R_{i1}^2	k_{i2}	R_{i2}^2
	(μg/mg $min^{0.5}$)		**(μg/mg $min^{0.5}$)**	
Adsorption in PBS				
H^+-PANI	60.74	----	4.68	0.939
H^+-PANI/SBA-15	55.26	0.971	3.15	0.926
Adsorption in water				
H^+-PANI	46.19	0.976	3.73	0.896
H^+-PANI/SBA-15	37.94	0.97	10.03	0.855

3. Further Study of Adsorption Properties of OG in H^+-PANI/SBA-15

The equilibrium and kinetic adsorption experiments were performed with initial OG concentration ranging from 50-500 μg/mL and adsorbent concentration of 1 mg/mL at room temperature. The results are compiled below.

3.1. Effect of initial concentration and contact time

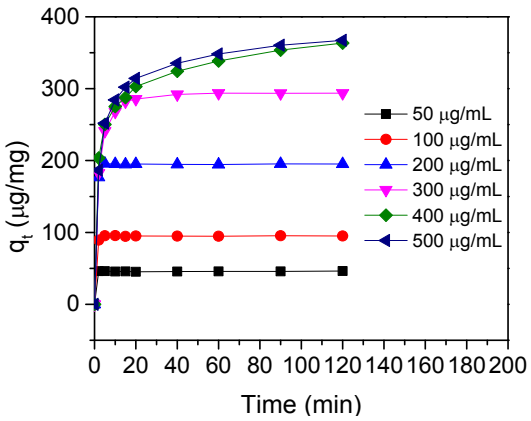

Fig. S17. Amount of OG adsorbed per unit mass of H^+-PANI/SBA-15 from solutions with different initial concentrations of OG.

Fig. S17 shows the variation of the amount of OG adsorbed on H^+-PANI/SBA-15 versus time from solutions with different initial concentrations of OG. It was observed that for OG solutions with initial concentrations between 50-200 μg/mL, the time needed to reach equilibrium was less than 10 min, while for higher initial OG concentration of 300-500 μg/mL, equilibrium could take as much as 2 h. To make sure that the full equilibrium was attained, the adsorption experiments were run for 6 h. This adsorption process can be explained as follows. First, the dye molecules encounter the outer surfaces of H^+-PANI/SBA-15 and get adsorbed there. They then get increasingly diffused into the

pores of the adsorbent. Thus, OG with higher initial concentration will take relatively longer contact time to reach an equilibrium point, as there are more molecules to diffuse into the pores, in a process that takes relatively longer time.

It can also been seen that the amount of OG adsorbed in H^+-PANI/SBA-15 expectedly increases with time; however, at some point it reaches a constant value where no additional OG can be adsorbed by the material. At this point, the amount of OG adsorbing into the material and desorbing from the material are said to be in a state of dynamic equilibrium. Similar phenomena are reported for the adsorption of other dyes and molecules, such as methylene blue on activated carbon prepared from coconut husk and tetracycline on NaOH-activated carbon produced from macadamia nut shells.[5,6]

3.2. Effect of pH

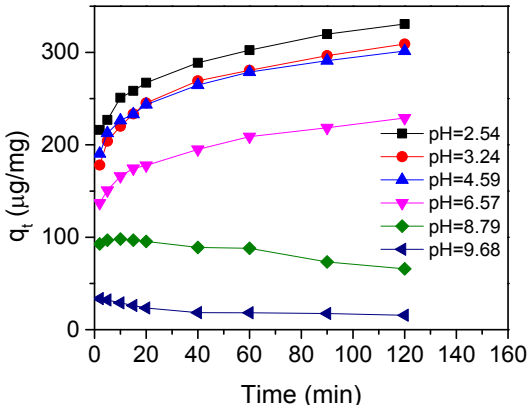

Fig. S18. Adsorption profiles of OG dye in the presence of H^+-PANI/SBA-15 at different pH values.

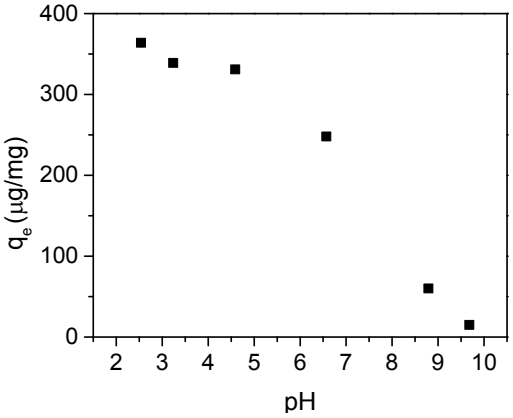

Fig. S19. The amount of OG adsorbed in H^+-PANI/SBA-15 at equilibrium versus the pH of the solution.

The pH of the solution plays an important role in the adsorption of OG, as shown in Fig. S18 and Fig. S19. The experiments were performed with a constant initial concentration of OG of 500 μg/mL. As can be seen in the results, the amount of OG adsorbed in the material decreases as the pH value of the solution increases (or vice versa). This phenomenon can be explained by the fact that lower pH makes the backbone of H^+-PANI/SBA-15 more positively charged, enhancing its ability to exert electrostatic attractions toward the negatively charged anionic OG adsorbate molecules. On the other hand, at higher pH (*e.g.*, pH 9.68), the amount of OG adsorbed in the material is negligible, which means most of the adsorbent is transformed to its emeraldine base form at this pH and is no longer able to pick up the OG molecules.[7]

3.3. Adsorption isotherms

Adsorption isotherms describe how the adsorbate molecules distribute between the liquid and solid phase when the system reaches equilibrium. Fitting experimental data into different isotherm models can give information about how adsorbate molecules interact with adsorbent surfaces.

The equilibrium adsorption isotherm of OG on H^+-PANI/SBA-15 is shown in Fig.

S20. At low OG concentrations, the graph shows a steep increase, indicating H^+-PANI/SBA-15' strong affinity toward OG molecules. However, at higher OG concentrations, the graph plateaus and the material is able to no longer adsorb more OG after a certain point (which means it reaches its adsorption capacity).

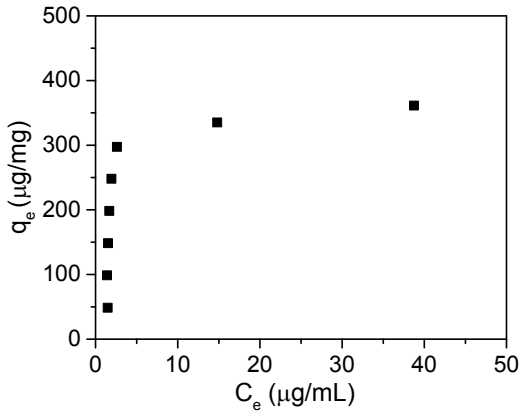

Fig. S20. Equilibrium adsorption isotherm of OG on H^+-PANI/SBA-15.

The isotherm models of Langmuir, Freundlich and Temkin were applied on the data, and the applicability of each model to describe the adsorption process is then judged by the value of its correlation coefficient values (R^2).

3.3.1. Langmuir isotherm

The Langmuir isotherm is given as following:[6]

$$q_e = \frac{q_m K_L C_e}{1 + K_L C_e} \qquad (8)$$

where q_e is the equilibrium solid phase adsorbate concentration (μg/mg), q_m is the maximum adsorption capacity (μg/mg), C_e is the equilibrium liquid phase adsorbate concentration (μg/mL), and K_L is the Langmuir adsorption constant (mL/μg). Equation (8) can be rearranged to the following linear form:

$$\frac{C_e}{q_e} = \frac{C_e}{q_m} + \frac{1}{K_L q_m} \qquad (9)$$

Thus, if the adsorption follows Langmuir isotherm, the plot of C_e/q_e versus C_e should be linear and the values of q_m and K_L can be determined from the slope and the intercept of the graph, respectively.

The dimensionless separation factor, R_L, is also an important parameter, which can indicate the favorability of the adsorption process. R_L is defined as:[6]

$$R_L = \frac{1}{1 + K_L C_0} \qquad (10)$$

where C_0 is the highest initial dye concentration (μg/mL) and K_L is the Langmuir constant. Based on the value of R_L, the adsorption process can be said to be irreversible ($R_L = 0$), favorable ($0 < R_L < 1$), linear ($R_L = 1$) or unfavorable ($R_L > 1$).

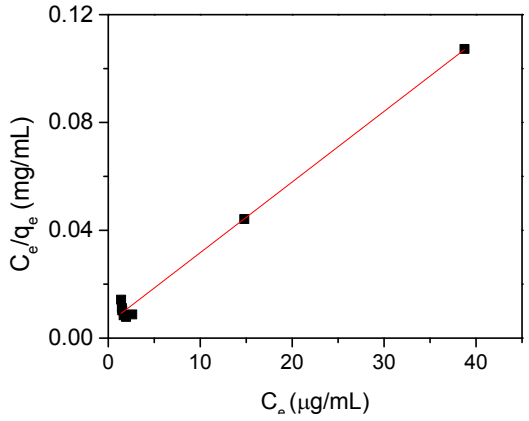

Fig. S21. A plot based on Langmuir isotherm of adsorption of OG on H^+-PANI/SBA-15.

As shown in Fig. S21, when C_e/q_e was plotted against C_e, a straight line was obtained, and the correlation coefficient R^2 was found to be 0.99, indicating the adsorption of OG on H^+-PANI/SBA-15 can be fitted well with the Langmuir isotherm. The corresponding values of q_m and K_L are calculated from equation (9) and compiled in Table S3. The separation factor R_L was found to be 0.004, which is in the range of 0-1; so, this again

confirms the favorable uptake of OG by H^+-PANI/SBA-15.

3.3.2. Freundlich isotherm

The Freundlich model, which is an empirical model that describes heterogeneous surfaces with sites of different affinities, can be written as:[6]

$$q_e = K_F C_e^{1/n} \quad (11)$$

where q_e is the equilibrium solid phase adsorbate concentration (μg/mg), C_e is the equilibrium liquid phase adsorbate concentration (μg/mL), K_F is the Freundlich constant (μg/mg)(mL/μg)$^{1/n}$ and n is the heterogeneity factor giving an indication of how favorable the adsorption process is.

By taking the logarithm of equation 11, a linear form of Freundlich expression can be obtained as follows:

$$ln\, q_e = ln\, K_F + \frac{1}{n} ln C_e \quad (12)$$

A linear plot of $ln\, q_e$ versus $ln\, C_e$ enables the constant K_F and n to be determined. The ratio of $1/n$ is a measure of surface heterogeneity, and as its value gets closer to zero, the material surface is said to be more heterogeneous.

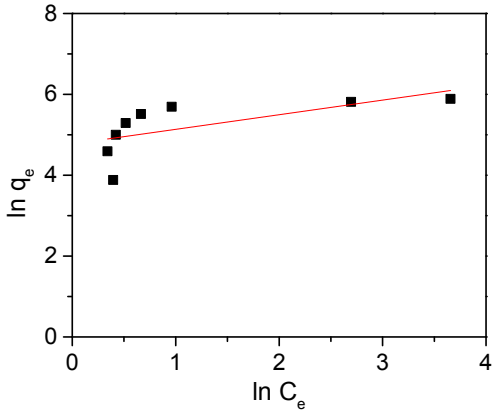

Fig. S22. Freundlich isotherm of OG on H^+-PANI/SBA-15

The plot of lnq_e versus lnC_e gave a straight line with a slope of 0.43, see Fig. S22,

from which the values of K_F and n were determined and compiled in Table S3.

3.3.3. Temkin isotherm

The Temkin model assumes that the heat of adsorption of all the molecules on the layer of the adsorbent would decrease linearly with the surface coverage due to adsorbate/adsorbent interactions.[5] The Temkin model can be used in the following form:

$$q_e = \frac{RT}{b} lnK_T + \frac{RT}{b} lnC_e \qquad (13)$$

where b is the Temkin constant related to the heat of adsorption (J/mol), K_T is the Temkin isotherm constant (L/g), R is the gas constant (8.314 J/mol K) and T the absolute temperature (K). Thus, a plot of q_e versus $ln\, C_e$ can be used to determine the values of b and K_T, from the slope and intercept of the graph, respectively, see Fig. S23 and Table S3.

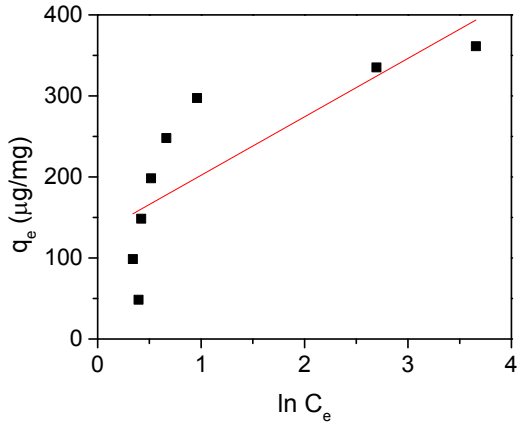

Fig. S23. Temkin isotherm of OG on H^+-PANI/SBA-15.

Table S3. Parameters obtained based on the Langmuir, Freundlich, and Temkin isotherm models.

Isotherm model	Parameters
Langmuir	Q_m = 384.61 μg/mg
	K_L = 0.47 mL/μg
	R^2= 0.99
Freundlich	K_F= 118.32 (μg/mg)(mL/μg)$^{1/n}$
	n = 2.766
	R^2= 0.43
Temkin	K_T = 6.06 L/g
	b= 34.61 J/mol
	R^2 = 0.64

Table S3 summarized all the constants and their corresponding correlation coefficients, R^2 for the three isotherm models. Among the three models, the Langmuir model was found to best fit the experimental data, giving R^2 = 0.99. Conformation of the experimental data into Langmuir isotherm equation indicates the homogeneous nature of H^+-PANI/SBA-15 surface and also that the OG molecule are distributed on the surface of H^+-PANI/SBA-15 in monolayers.

Table S4. Comparisons based on q_m values (the maximum adsorption capacity of adsorbents) of different adsorbents applied for removal of OG from solutions.

Material (Adsorbent)	q_m (mg/g)	Reference
PVA@SiO1.5-hPEA-1/2-Gel [a]	4.57 (ca.)	8
rGO [b]	5.98	9
Activated carbon from Thespesia populnea pods	9.129	10
BFA [c]	18.796	11
MAMPS, MAMMS [d]	48.98; 61.33	12
DTCSCu [e]	53.38	13
Nano zirconia	54.31±1.573 (ca.)	14
LDH, CLDH [f]	76.4; 378.8	15
HDTMAB [g]	101.42 (ca.)	16
Chitosan (ungrafted), ChgPHMA, ChgPBMA, ChgPEMA, ChgPMMA [h]	95; 265; 290; 360; 435	17
H^+-PANI/SBA-15	***384.61***	***Present work***
Chitosan	922.9	18
Chitosan/DTAC [i]	1452.07	19

[a] PVA@SiO1.5-hPEA-1/2-Gel = Poly(vinyl alcohol) (PVA)-enhanced hybrid hydrogels of hyperbranched poly(ether amine) ($SiO_{1.5}$-hPEA-Gels). [b] rGO = Reduced graphene oxide. [c] BFA = Bagasse fly ash. [d] MAMMS = Monoamine-modified magnetic silica and MAMMS = Magnetite-free MAMMS. [e] DTCSCu = Copper(II) complex of dithiocarbamate-modified starch. [f] LDH = Layered double hydroxide; CLDH = Mg–Fe layer double hydroxide. [g] HDTMAB = Na-bentonite modified with hexadecyltrimethylammonium bromide. [h] ChgPHMA = Chitosan grafted poly(hexyl methacrylate); ChgPBMA = Chitosan grafted poly(butyl methacrylate); ChgPEMA = Chitosan grafted poly(ethyl methacrylate); ChgPMMA = Chitosan grafted poly(methyl methacrylate). [i] Chitosan/DTAC = Chitosan/Dodecyltrimethylammonium chloride.

3.4. Adsorption kinetics

To get a further understanding of the adsorption processes, the data for the adsorption of OG on H^+-PANI/SBA-15 obtained at different initial OG concentration were fitted with pseudo-second order and intraparticle diffusion models (Fig. S24 and Fig. S25), and the corresponding fitting values are compiled in Table S5 and Table S6.

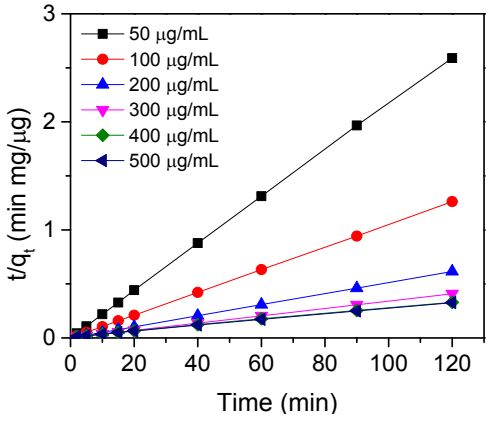

Fig. S24. Plots based on pseudo-second order model of the adsorption of OG by H^+-PANI/SBA-15 from solutions with different initial OG concentrations.

Table S5. Kinetic data of Pseudo-second order model of OG adsorption by H^+-PANI/SBA15 with different initial OG concentrations.

OG Concentration	**Second order kinetic model**			
(μg/mL)	q_e **(exp)**	k_2	q_e **(cal)**	R^2
	(µg/mL)	**(mg/µg min)**	**(µg/mL)**	
50	46.33	9.42 x 10^{-2}	46.08	1
100	95.09	1.84 x 10^{-1}	95.24	1
200	195.19	6.5 x 10^{-2}	196.08	1
300	293.71	3.61 x 10^{-3}	294.12	0.999
400	363.48	7.44 x 10^{-4}	370.3	0.999
500	367.18	8.38 x 10^{-4}	377.36	1

From Figure S24 and Table S5, for initial OG concentration varied from 50-500 μg/mL, pseudo-second order kinetic model all showed great agreement between the experimental and the calculated q_e values. In addition, the correlation coefficient, R^2, was found to be greater than 0.999 for all these cases, confirming that the pseudo-second order kinetic model was applicable to describe the adsorption behavior of OG on H^+-PANI/SBA-15.

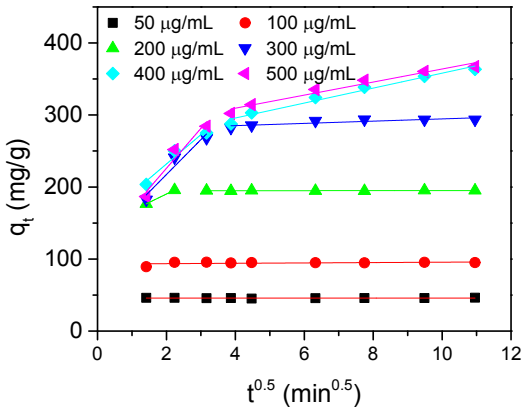

Fig. S25. Plots based on intraparticle diffusion model of the data of adsorption of OG by H^+-PANI/SBA-15 from solutions with different initial OG concentrations.

Table S6. Kinetic data obtained based on intraparticle diffusion model of the data of adsorption of OG by H^+-PANI/SBA15 in distilled water.

OG Concentration	**Intraparticle diffusion model**			
(μg/mL)	k_{i1}	R^2	k_{i2}	R^2
	(μg/mg $min^{0.5}$)		**(μg/mg $min^{0.5}$)**	
50	0.01	0.22	----	----
100	0.25	0.38	----	----
200	0.84	0.4	----	----
300	48.44	0.941	1.56	0.751
400	40.63	0.957	10.38	0.975
500	55.43	0.949	9.07	0.965

It can be observed from Figure S25 and Table S6 that at lower initial OG concentration, only one adsorption step on the plot of q_t versus $t^{0.5}$ was observed. However, at higher initial OG concentration, the plot of q_t versus $t^{0.5}$ was not linear in the whole range, and it could be separated into two linear sections, indicating the presence of multistage adsorption process. The first linear region was attributed to the diffusion of OG on the external surfaces of H^+-PANI/SBA-15, and its high k_{i1} value demonstrated that the processes were fast due to the strong electrostatic interaction. The second portion could be ascribed to the gradual adsorption of OG, controlled by the intraparticle diffusion, and in this stage, the OG molecules entered the porous structure of the adsorbents. Furthermore, the linear plots did not pass through the origin, suggesting that the adsorption process was not only controlled by intraparticle diffusion, but instead was dictated by both external mass diffusion and intraparticle diffusion processes.[5,6,19,20]

3.5. Thermodynamic studies

The effect of temperature on OG adsorption on H^+-PANI/SBA-15 was studied at 20, 30 and 40 °C with constant initial OG concentration of 500 μg/mL and an adsorbent concentration of 1 mg/mL, see Figure S26. From the results, the activation energy (E_a), Gibbs free energy (ΔG°), enthalpy (ΔH°) and entropy (ΔS°) of the adsorption processes were also calculated (see below).

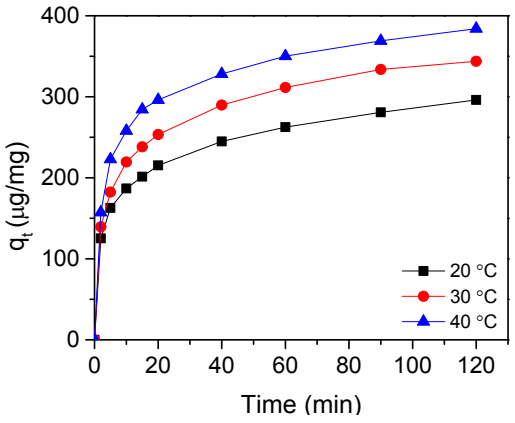

Fig. S26. Effect of temperature on removal of OG by H^+-PANI/SBA-15.

From Figure S26, it can be seen that an increase in temperature causes a slight increase in the amount of OG adsorbed by H^+-PANI/SBA-15, suggesting the adsorption process of OG on H^+-PANI/SBA-15 is endothermic.

3.5.1. Activation energy (E_a)

The magnitude of activation energy can be used to determine whether the adsorption of a given compound on a given adsorbent takes place *via* physical or chemical process. Physisorption process has usually activation energy values ranging from 5-40 kJ/mol, whereas chemisorption has a relatively higher activation energy range between 40-800 kJ/mol.[20] To get the value of the activation energy, Arrhenius equation was used:

$$ln\, k_2 = ln\, A - \frac{E_a}{RT} \qquad (14)$$

where k_2 is the pseudo second order rate constant of OG adsorption, E_a is the Arrhenius energy (kJ/mol), A is the Arrhenius factor, R is the gas constant (8.314 J/mol K) and T is the absolute temperature of the solution (K). A straight line with slope $-E_a/R$ was obtained upon plotting $ln\, k_2$ versus $1/T$ (see Figure S27). The activation energy (5.55 kJ/mol) is tabulated with other thermodynamic parameters in Table S7. The result confirms that the adsorption of OG on H^+-PANI/SBA-15 occurs *via* physisorption.

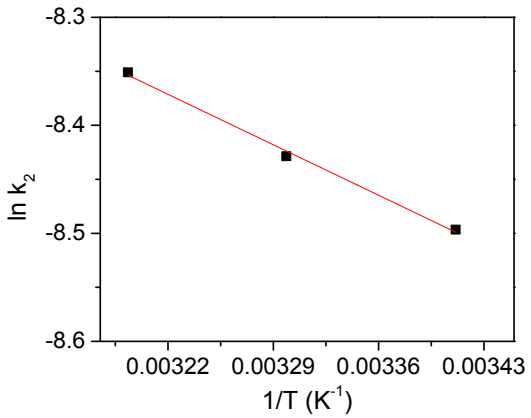

Fig. S27. A plot of $ln\, k_2$ vs. $1/T$ for the data of adsorption of OG on H^+-PANI/SBA-15.

3.5.2 Gibbs free energy (ΔG°), enthalpy (ΔH°) and entropy (ΔS°)

Thermodynamic parameters, namely ΔG°, ΔH° and ΔS°, for the adsorption processes of OG on H^{+}-PANI/SBA-15 were determined from equation (15), (16) and (17):

$$k_c = \frac{q_e}{C_e} \; and \; \Delta G^{\circ} = -RT ln \, k_c \qquad (15)$$

$$\Delta G^{\circ} = \Delta H^{\circ} - T\Delta S^{\circ} \qquad (16)$$

$$ln k_c = -\frac{\Delta H^{\circ}}{RT} + \frac{\Delta S^{\circ}}{R} \qquad (17)$$

where k_c is the standard thermodynamic equilibrium constant (mL/mg), q_e is the equilibrium solid phase adsorbate concentration (μg/mg), C_e is the equilibrium liquid phase adsorbate concentration (μg/mL), R is the gas constant (8.314 J/mol K), and T is the absolute temperature of the solution (K). The values of ΔH° and ΔS° can be estimated from the slope and intercept after plotting $ln \, k_c$ versus $1/T$ (Fig. S28). The values of thermodynamic parameters are listed in Table S7. The positive value ΔH° indicates that the adsorption process of OG on H^{+}-PANI/SBA-15 is endothermic while the negative value of ΔG°, which decreased with an increase of temperature, reveals the spontaneity of the adsorption process. The value of ΔG°, which ranged from -1.88 to -4.51 kJ/mol, once again confirming the physisorption process (-20 to 0 kJ/mol).[21] Similar results have been reported for the adsorption of other dyes such as acid green 25 and brilliant blue R on adsorbents such as activated palm ash[20] and organo-attapulgite (ATPOC) and organo-bentonite (BNTOC) clay-based materials.[21] The positive value of ΔS° suggests the increased randomness at the solid-solution interface during the adsorption process, and this phenomenon has also been described by other researchers.[5,20,21]

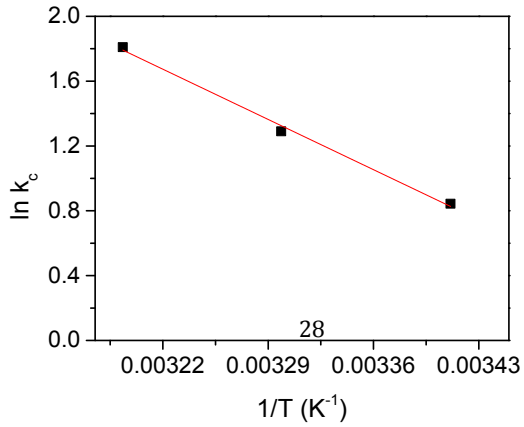

Fig. S28. A plot of $\ln k_c$ vs. $1/T$ for the data of adsorption of OG on H^+-PANI/SBA-15.

Table S7. Thermodynamic data for adsorption of OG on H^+-PANI/SBA-15.

E_a	ΔH°	ΔS°	ΔG° (kJ/mol)		
kJ/mol	**kJ/mol**	**kJ/mol**	**20** ℃	**30** ℃	**40** ℃
5.55	36.82	0.132	-1.88	-3.2	-4.51

3.6. Regeneration

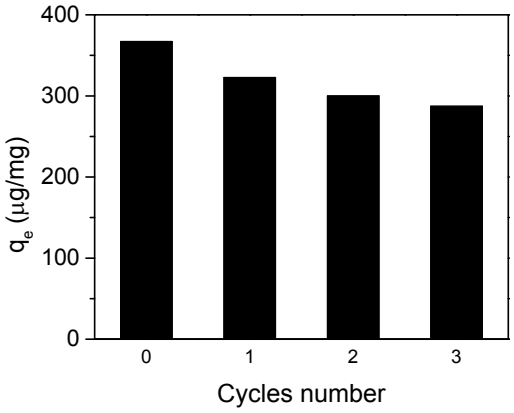

Fig. S29. Adsorption amount of OG on H^+-PANI/SBA-15 and on recovered and regenerated H^+-PANI/SBA-15 materials. In the experiments, the initial concentration of OG was 500 μg/mL and the adsorbent concentration was 1 mg/mL.

As shown in Figures S18 and 19, the amount of OG adsorbed on H^+-PANI/SBA-15 decreased as the pH of the solutions increased, implying that the adsorbate molecules loaded on the adsorbent can be desorbed. To perform the regeneration test, the pre-loaded

adsorbent was re-dispersed into $NaHCO_3$ solution and stirred vigorously for 30 min, this washing process was repeated twice to make sure that most of the adsorbed OG was desorbed from the adsorbent. The desorbed PANI/SBA-15 was then centrifuged and washed three times with water and re-doped with hydrochloric acid. The regenerated adsorbent was used again in the subsequent experiments of OG adsorption. From Figure S29, it was observed that at first cycle, the OG adsorption amount reduced from 367.17 μg/mg to 322.78 μg/mg, but in the next two adsorption-desorption cycles, there was only slight decrease in the final adsorbed amount of OG. This proved that H^+-PANI/SBA-15 could be used repeatedly without significantly losing its adsorption properties and adsorption capacity.

References for Supporting Information

1 S. Weng, Z. Lin, Y. Zhang, L. Chen, J. Zhou, *React. Funct. Polym*., 2009, **69**, 130.

2 M. M. Ayad, A. A. EI-Nasr, *J. Phys. Chem. C*., 2010, **114**,14377.

3 C. Namasivayam, D. Kavitha, *Dyes Pigm*., 2002, **54**, 47.

4 W. J. Weber, J. C. Morris, *J. Sanit. Eng. Div. Am. Soc. Civ. Eng.* 1963, **89**, 31.

5 I. A. W. Tan, A. L. Ahmad, B. H. Hameed, *J. Hazard. Mater.*, 2008, **154**, 337.

6 A. C. Martins, O. Pezoti, A. L. Cazetta, K. C. Bedin, D. A. S. Yamazaki, G. F. G. Bandoch, T. Asefa, J. V. Visentainer, V. C. Almeida, *Chem. Eng. J.*, 2015, **260**, 291

7 D. Mahanta, G. Madras, S. Radhakrishnan, S. Patil, *J. Phys. Chem. B.*, 2009, **113**, 2293.

8 S. J. Deng, H. J. Xu, X. S. Jiang, J. Yin, *Macromolecules*., 2013, **46**, 2399.

9 G. K. Ramesha, A. Vijaya Kumara, H. B. Muralidhara, S. Sampath, *J. Colloid Interface Sci.*, 2011, **361,** 270.

10 M. Arulkumar, P. Sathishkumar, T. Palvannan, *J. Hazard. Mater.*, 2011, **186**, 827.

11 I. D. Mall, V. C. Srivastava, N. K. Agarwal, *Dyes and Pigments.*, 2006, **69**, 210.

12 A. A. Atia, A. M. Donia, W. A. A. Amrani, *Chem. Eng. J.*, 2009, **150**, 55.

13 R. M. Cheng, S. J. Ou, B. Xiang, Y. J. Li, Q. Q. Liao, *Langmuir*., 2010, **26**, 752.

14 Y. C. Sharma, D. Gusain, S. N. Upadhyay, *RSC. Adv.,* 2014, **4**, 18755.

15 N. Benselka-Hadj. Abdelkader, A. Bentouami, Z. Derrichea, N. Bettahar, L. C. de Ménorval, *Chem. Eng. J.*, 2011, **169**, 231.

16 N. Jović-Jovičić, A. Milutinović-Nikolić, P. Banković, Z. Mojović, M. Žunić, I. Gržetić, D. Jovanović, *Appl. Clay Sci.*, 2010, **47**, 452.

17 V. K. Konaganti, R. Kotaa, S. Patil, G. Madras, *Chem. Eng. J.*, 2010, **158**, 393.

18 Y. C. Wong, Y. S. Szeto, W. H. Cheung, G. McKay, *Langmuir*., 2003, **19**, 7888.

19 L. Zhang, Z. Cheng, X. Guo, X. Jiang, R. Liu, *J. Mol. Liq.*, 2014, **197**, 353.

20 B. H. Hameed, A. A. Ahmad, N. Aziz, *Chem. Eng. J.*, 2007, **133**, 195.

21 A. S. Bhatt, P. L. Sakaria, M. Vasudevan, R. R. Pawar, N. Sudheesh, H. C. Bajaj, H. M. Mody, *RSC Adv*., 2012, **2**, 8663.